International Journal of Naval Architecture and Ocean Engineering 14 (2022) 100461

Contents lists available at ScienceDirect

International Journal of Naval Architecture and Ocean Engineering

journal homepage: http://www.journals.elsevier.com/international-journal-of-naval-architecture-and-ocean-engineering/

Numerical investigation of depth-varying currents on ship hydrodynamics in confined water

Momchil Terziev [a, *], Tahsin Tezdogan [b], Yigit Kemal Demirel [b], Claire De Marco Muscat-Fenech [c], Atilla Incecik [a]

[a] Faculty of Engineering, University of Strathclyde, Glasgow, UK
[b] Department of Naval Architecture, Ocean and Marine Engineering, University of Strathclyde, Glasgow, UK
[c] Faculty of Engineering, University of Malta, Msida, Malta

ARTICLE INFO

Article history:
Received 24 March 2022
Received in revised form
3 May 2022
Accepted 16 May 2022
Available online 26 May 2022

Keywords:
KCS
URANS
Sheared currents
Confined water
Ship resistance
CFD

ABSTRACT

Vessels can operate in unpredictable environments depending on the geographical area and weather conditions. One example of conditions a vessel might not be assessed against is the presence of depth-varying currents, which are particularly relevant in confined waters where currents can be created due to tidal influences, or short fetches in inland waterways. The possible presence of depth-varying currents motivates a numerical assessment of the effects of sheared currents on the hydrodynamic performance of the KRISO Container Ship (KCS) in confined waters. The results highlight that exploiting currents, such as those generated by tides could be used to improve the energy efficiency of vessels considerably. These currents present significant possibilities for voyage optimisation based on geographical and meteorological conditions. The results specific for the KRISO container ship point to resistance reductions when the current assists ship motions, accompanied by considerable decreases in sinkage and trim. Conversely, when currents oppose ship motion, resistance, sinkage and trim can increase by a factor of 3 depending on the strength and shape of the depth-varying current. The results also show that a current with constant vorticity, a case frequently used in the literature to investigate the impact of sheared currents, creates the biggest increase and decrease for inhibiting and assisting currents, respectively.

© 2022 Society of Naval Architects of Korea. Production and hosting by Elsevier B.V. This is an open access article under the CC BY license (http://creativecommons.org/licenses/by/4.0/).

1. Introduction

The study of ship resistance is a rich and diverse field, comprising a multitude of methods and approaches. In recent years, Reynolds Averaged Navier-Stokes (RANS) methods have emerged as the dominant approach in the field. The advent of such methods has allowed virtually every conceivable aspect of numerical ship resistance prediction to be investigated with the aim to understand a ship's operational performance and the conditions it may be subject to (De Luca et al., 2016; Elsherbiny et al., 2019; Kok et al., 2020; Mucha et al., 2016; Terziev et al., 2019).

It is of critical importance to accurately model the environmental conditions a ship will sail in. Otherwise, the performance of the ship will be misrepresented at the design stage, potentially leading to the ship's inability to satisfy contractual obligations. An area of interest from a hydrodynamic perspective is the impact of shear currents, that is, depth-varying currents, on ship performance. Ekman (1905) showed the oceanic surface moves along spiral motions, suggesting vessels are almost always subjected to a current. Such currents can also be generated as a result of tidal action in shallow seas or long canals. Alternatively, the natural flow or rivers, or the short fetch of many inland waterways may be responsible for the creation of currents. Vessels operating in confined waterways subject to tidal influences may optimise the departure and arrival time based on the tide to enhance energy efficiency presenting new opportunities for scheduling optimisation. To the best of the authors' knowledge, such effects have not been investigated previously.

The work presented here aims to investigate the influence of sheared currents on ship hydrodynamics in confined water using the commercially available Computational Fluid Dynamics (CFD) solver, Star-CCM+, version 15.06.007. Making use of a RANS approach has several benefits. Specifically, RANS methods are fully non-linear and include viscous effects within the solution, which

* Corresponding author.
E-mail address: momchil.terziev@strath.ac.uk (M. Terziev).
Peer review under responsibility of The Society of Naval Architects of Korea.

https://doi.org/10.1016/j.ijnaoe.2022.100461
2092-6782/© 2022 Society of Naval Architects of Korea. Production and hosting by Elsevier B.V. This is an open access article under the CC BY license (http://creativecommons.org/licenses/by/4.0/).

allows one to obtain a useful estimate of the total resistance change when compared to still water.

The remainder of the work is organised as follows. The next section details the background and past research on sheared currents and ship hydrodynamics in confined water. Then, the numerical set up and case studies are detailed. Following this, an example case is validated against available experimental results. Additionally, a number of case studies are presented to investigate the importance of sheared currents. Finally, conclusions and recommendations for future work are given in the last section.

2. Background

Historically, the study of wave-current interactions has been motivated by the resulting modifications to ocean wave spectra (Skop and Leipold, 1988; Yoshida, 1952). These in turn influence the design of offshore and coastal structures (Skop, 1987). A plethora of studies have examined such phenomena, but Ekman (1905) appears to have ignited interest in the field by showing that the oceanic surface follows a spiral motion.

Thompson (1949) showed the dispersion relation of a case where waves interact with a current may be found using the kinematic surface condition at the water surface. Around the same time, Abdullah (1949) found the dispersion relation of waves interacting with an exponentially varying current. Burns (1953) obtained an integral expression describing the dispersion relation. In an appendix to Burns' (1953) work, Lighthill presented results including the effect of surface tension for a case where the depth-varying current changes according to a 1/7 power law. The same case was examined by Hunt (1955), who abandoned the long wave theory used by earlier researchers in favour of a more general set-up.

Early studies into wave-current interactions showed that waves may be stopped, or wave breaking may be induced by a current. Such studies are reported by, for example, Taylor (1955), who studied the effect of the bubble-generated current on waves and its wave stopping ability motivated by Evans' (1956) experimental work.

Longuet-Higgins and Stewart (1960) carried out an evaluation of Stokes waves to second order, modifying Unna's (1947) formations. According to Peregrine (1976), Longuet-Higgins and Stewart (1960, 1961) were first to give an adequate theoretical framework of waves propagating over a current. They introduced the concept of radiation stress (and corresponding radiation stress tensor), which describes the additional momentum flux generated by the presence of waves on a current. In a series of papers, Longuet-Higgins and Stewart (1960, 1961, 1962) fully analysed wave-current interactions. Subsequently, a summary paper was presented (Longuet-Higgins and Stewart, 1964), where the method was extended to capillary effects.

Bretherton and Garret (1968) demonstrated that changes in linear, irrotational wave amplitude and corresponding energy along a ray can be computed through the conservation of wave action. Crapper (1972) compared the linear method of Longuet-Higgins and Stewart (1960, 1961, 1962) with his non-linear formulation and that found lesser rates of wave amplitude growth are predicted as a result of including higher order terms. A further investigation on non-linear waves on a current was performed by Holliday (1973), who found that finite wave amplitude effects are stronger for gravity waves. He also showed that Gargett and Hughes' (1972) "wave barrier" problem is overcome by considering the aforementioned effects in a non-linear framework.

Up to this point, studies investigating the general case of free waves propagating over a current were reviewed. It is now useful to introduce the vorticity parameter (S) and shift focus to ship-generated waves investigations. In linear shear currents, or equivalently, currents of constant vorticity, the flow may be described as shown in Eq. (1).

$$U(d) = U_0 + S(d - h) \tag{1}$$

where $U(d)$ is the depth-varying flow velocity in m/s, U_0 is the velocity at the water surface in m/s, $S = U_0/h$ with h being the water depth measured in m^{-1}, d is the wall distance in m. This nomenclature partially is adopted from Ellingsen and Brevik (2014). The reasons of using of the wall distance are explained in the following section.

To the best of the authors' knowledge, Tatinclaux (1970) was first to investigate the effects of vorticity on ship waves in deep waters, focussing on the wake generated by the ship rather than a background current. Specifically, Tatinclaux (1970) studied the effect of the accelerated mass of water a ship pulls along its track on the generation of waves from the ship's stern, which acts like a sheared current. By showing that the stern is a weaker source of waves due to the current it operates in, Tatinclaux (1970) motivated Peregrine (1971) to derive a relationship between the wavelengths produced by the stern in the wake-induced flow and the bow diverging wave system.

Around the same time, Beck (1971) considered the problem of a ship's wake as a region with vorticity. The approach used by Beck (1971) allowed the aforementioned region to retain the action of viscosity in the linear thin-ship mathematical framework used. In contrast to Beck's (1971) approach of distributing vortex sheets in the wake, Brard (1970) and Tatinclaux (1970) used a continuous distribution of vorticity in the wake. The main finding from Beck's (1971) work is that a wake-wake interaction term (in the absence of a background current) can have an either positive or negative effect on a ship's wave resistance, where it may contribute up to about 10% to the wave resistance force on a ship.

While the abovementioned studies contributed significantly to the understanding of ship resistance, the effect of a background sheared current on ship hydrodynamics was not modelled. In fact, to the best of the authors' knowledge, this was only done recently for deep and shallow water cases (Aalvik, 2019; Benzaquen et al., 2014; Ellingsen, 2014; Li et al., 2019; Li and Ellingsen, 2016a, 2016b). Some interesting findings from these recent studies include that a ship's resistance may differ by a factor of 3 depending on whether the current is assisting or inhibiting ship motion. Ellingsen (2014) solved the linear ship wave problem in deep waters, showing that a shear current acting on the wave system can alter the Kelvin wake angle depending on the current strength and direction relative to the vessel's. Ellingsen and Brevik (2014) developed a two-dimensional theory of waves propagating on flow of uniform vorticity, while Li and Ellingsen (2016a) performed the first wave resistance calculations for a ship advancing atop a sheared current. Li et al. (2019) devised a mathematical theory to obtain the transient wave resistance of a vessel using the current from the Colombia river as a benchmark. Aalvik (2019) explored how the speed and depth affect the mathematical representation of a hull as a pressure distribution in calm water and when subject to a depth-varying current.

As demonstrated in this section, the importance of vorticity on ship waves has been recognised by many researchers. It is now appropriate to shift focus to Navier-Stokes-based investigations of ship hydrodynamics in shallow and confined water.

Tabaczek (2008) used the Fluent solver to model the resistance of a barge in depth-to draught ratios of 1.176–2. Satisfactory agreement was found between numerical results and experimental data. The error was generally shown to increase with speed in the shallowest case at a faster rate than in deeper water. Castiglione

et al. (2014) investigated shallow water effects on the interference of a catamaran in shallow water depth-to-draught ratios between 8.2 and 2 at subcritical and supercritical speeds. The findings of Castiglione et al. (2014) include that shallow water intensifies the interference effect with respect to deep water, causing increased resistance. Here, subcritical speeds refer to cases when the depth Froude number is smaller than 1 ($Fr_h = U/\sqrt{gh} < 1$, where U is the ship speed in m/s, g is the gravitational acceleration, and h is the water depth in m).

Chun et al. (2001), Sakamoto et al. (2007), and Prakash and Chandra (2013) studied the differences in flow and resistance induced by shallow water. They found significant variations in all parameters induced by changes in the water depth or the depth-to-draught ratio. More recently, Rotteveel et al. (2017) showed that propulsive power requirements in shallow water can be decreased at the cost of increased propulsion power requirements in deep water, indicating at the varying flow physics governing each case. Razgallah et al. (2018) modelled the impact of free surface modelling on hydrodynamic forces of a vessel in shallow water. Findings from the aforementioned study indicate that free surface modelling becomes important and should not be neglected at a drift angle of no more than 3 °. Similarly, with increasing speed, the importance of modelling the free surface increases.

Zeng et al. (2018) modified the ITTC57 line in an attempt to account for shallow water effects. Then, Zeng et al. (2019) presented shallow water friction lines for three hulls based on viscous resistance data obtained from CFD. Terziev et al. (2021) used the modified friction line given by Zeng et al. (2019) for the KCS and compared results in a canal, finding that some difference due to the confined width is present.

Mucha et al. (2016) carried out numerical validation exercises on shallow water performance and ship-bank interaction of three benchmark vessels, a subject also studied by Yao et al. (2011). Mucha et al. (2016) compared numerical results to experimental data, predictions from slender-body flow theory (Tuck, 1966), and a Rankine source method (Söding et al., 2012; Graefe et al., 2015). The key outcome of the work carried out by Mucha et al. (2016) is that all methods are generally capable of predicting ship hydrodynamics in confined water well. In very shallow water, the RANS solution exhibited turbulence and near-wall modelling dependence. Terziev et al. (2020) compared widely used turbulence models as applied to confined water cases, where it was identified that for low y^+ meshes, the k-ω model was the best choice for resistance, sinkage, and trim.

More recently, Bechthold and Kastens (2020) investigated the ability of a URANS method to model ship squat at depth-to-draught ratios smaller than 1.2. They found that although sinkage was predicted with good accuracy in almost all cases, a systematic overprediction of trim was present in the numerical results when compared to experimental data.

Although numerous studies investigate ship hydrodynamics in confined waters, to the best of the authors' knowledge no study has performed a RANS-based assessment of sheared current effects on ship performance. This paper aims to fill this gap in the literature by performing a study on the effects of sheared currents on ship hydrodynamics, with focus on calm, confined water resistance.

3. Case studies

This section provides information on the selected case studies and ship geometry. To begin with, a set of case studies are performed in the absence of a sheared current. This is done to enable a validation and verification exercise using the experimental data of Elsherbiny et al. (2019). Following the comparison with the experiment, a set of sheared currents are incorporated within the simulation on the same set-up (explained in the following section). It should be noted that the experimental data of Elsherbiny et al. (2019) used for validation purposes do not contain the effect of a depth-varying current. The particulars of the ship, the KRISO Container Ship (KCS) used in the experiment of Elsherbiny et al. (2019) and in the numerical simulations performed herein are given in Table 1.

The conditions under which the KCS is tested also follow the work of Elsherbiny et al. (2019). Once the validation and verification exercise is performed for the selected speed without a shear current, a set of sheared currents are included in the computational environment. The first current type is given by Eq. (1) (linear current, or constant vorticity, S), the second takes a 1/7th power law shape, as shown in Eq. (2), while the third type of current has an exponential form, given in Eq. (3), adapted from Ellingsen and Li (2017):

$$U(d) = U_0(d/h)^{1/7} \tag{2}$$

$$U(d) = \alpha\sqrt{gh}\exp(20d/h) \tag{3}$$

where d is the wall distance, and α is a constant whose value is chosen to produce a current of a specific strength at the free surface. The values of α for each investigated ship speed and current strength are obtained according to Eq. (4). For both depth Froude numbers investigated, U_0 is set to 30%, 20%, and 10% of the ship speed, resulting in the test matrix given in Table 2.

$$\alpha = F_h U_0 \Big/ U_{ship} \tag{4}$$

The current profile described by Eq. (2) is realistic for cases where tidal influences or natural river flow has caused the current. On the other hand, Eq. (1) and Eq. (3) may be more representative of cases where the current is wind driven if the fetch of a waterway is insufficient to generate wind waves. In all cases, U_0/U_{ship} determines the flow velocity at the free surface, allowing an assessment of the effect of a change in the depth-varying shape of the current. The wall distance is used in all cases to enable the flow to vary not only from the canal bottom, but also from the canal side.

To determine the potential for reduction in resistance as a result of assisting currents, the case studies include both inhibiting currents and assisting currents. The current is superposed onto the flow velocity of the vessel, as described in the following sections.

Other experimental datasets in shallow or confined water may be found in Eloot et al. (2016) Zwijnsvoorde et al. (2018) for the Duisburg container carrier. Validation research on such data was conducted by Mucha et al. (2016). The vessel chosen for the present investigation has also been subject to experimental investigations, such as that presented by Choi et al. (2019).

Table 1
Principal dimensions of the KCS model.

Quantity	Symbol	Value	Unit
Scale factor	Λ	75	–
Length	L	3.067	m
Beam	B	0.429	m
Draught	T	0.144	m
Depth	D	0.253	m
Block coefficient	CB	0.651	–
Wetted area	S	1.694	m^2
Depth Froude numbers tested	Fr_h	**0.303**[a], 0.47	–
Depth-to-draught ratio	h/T	2.22	–

[a] Chosen for validation and verification.

Table 2
Case studies modelled using CFD.

Current	Equation number	U_0/U_{ship}	F_h
None	–	0	0.303
Linear	Eq. (1)	0.1	
		0.2	
		0.3	
1/7 power law	Eq. (2)	0.1	
		0.2	
		0.3	
Exponential	Eq. (3)	0.1	
		0.2	
		0.3	
None	–	0	0.47
Linear	Eq. (1)	0.1	
		0.2	
		0.3	
1/7 power law	Eq. (2)	0.1	
		0.2	
		0.3	
Exponential	Eq. (3)	0.1	
		0.2	
		0.3	

4. Methodology

Up to this point, this work has focused on the background to the study. This section will provide details on the chosen methodology and its implementation.

4.1. The numerical environment

As stated in the introduction, the commercially available CFD solver, Star-CCM+, version 15.02.006 is employed. The solver makes use of a finite volume method which relies on the integral form of the governing equations and subdivides the computational domain into a finite number of adjoining cells.

The turbulence model chosen for this work is the standard k-ω Wilcox model (Wilcox, 2008) as implemented in the CFD solver (Siemens, 2018). The k-ω model is chosen based on results shown in Terziev et al. (2020), where the model's accuracy was investigated for problems similar to those examined herein. Moreover, the k-ω model was shown to be up to 16% more computationally efficient in terms of time per iteration when compared to other 2-equation eddy-viscosity turbulence models (Terziev et al., 2020). To ensure accurate representation of turbulent properties, all discretisation terms are set to second order accuracy.

4.1.1. Computational domain

The current sub-section contains detailed information pertaining to the dimension, boundary conditions and motion of the computational domain.

The computational domain is created according to accepted norms and recommendations of the International Towing Tank Conference (ITTC, 2014). To ensure that boundaries located in upstream and downstream of the ship do not influence the solution, they are placed at 2.5 ship lengths from the nearest perpendicular (forward and aft perpendicular, respectively). The total length of the computational domain is therefore 6 ship lengths ($L =$ 3.067 m). The lateral distance from the ship centreline to the side boundary is dictated by the experiment (Elsherbiny et al., 2019), namely 2.3 m. The water depth is kept constant, equal to 0.32 m, also set to match the experiment in all cases. Half of the domain is modelled to reduce the computational resources used, therefore, a symmetry plane is placed coincident with the ship and canal centreline. Finally, the domain top is placed 1.5 ship lengths from the undisturbed free surface in the z direction as shown in Fig. 1.

4.1.1.1. Boundary conditions. It is of critical importance to ensure that boundary conditions reflect the physics which a simulation attempts to approximate. In all cases, the domain bottom and side boundary conditions are set as no-slip walls. The vessel remains stationary in the x-direction, while the fluid is prescribed a velocity equal and opposite to that of the hull in the experiment. The ship velocity is also applied to the side and bottom boundaries so that in the ship's frame of reference, the fluid and domain walls move downstream. Velocity inlet and pressure outlet conditions are imposed on the upstream and downstream boundaries, respectively.

The inlet boundary introduces the prescribed current in addition to the ship velocity, while the outlet maintains the hydrostatic pressure to prevent backflow. To accelerate the convergence of the results numerical damping is applied, extending a distance equal to one ship length in the boundary normal direction. Numerical damping is only applied to the outlet and inlet boundaries to prevent interference with the physics of the solution. The resulting computational domain and boundary conditions are depicted in Fig. 1.

4.1.2. Mesh generation

The computational mesh is generated within the automatic facilities of Star-CCM+. A set of refinements around the free surface and vicinity of the ship are implemented to ensure an accurate representation of the physical phenomena. It should be noted that grid properties do not change across the examined case studies.

4.1.2.1. Near-wall mesh. The generation of a suitable mesh at no-slip boundaries is of critical importance to obtain an accurate value for the resistance of a ship. In all cases, a high y^+ strategy is adopted, where y^+ is in the range 30−110 depending on the value of $\mathrm{Fr_h}$ and U_0. Visual representations of computational mesh are shown in Fig. 2, while total cell numbers were approximately 4,770,598.

4.1.3. Time step selection

To ensure the solution is re-recreated well within the virtual environment of Star-CCM+, one must ensure an adequate time step is chosen. Temporal discretisation is set to 1st accuracy for all simulations. The value of the time step is set to $\Delta t = 0.0035\ \mathrm{L}/U_c$ following Terziev et al. (2018), where U_c is the maximum velocity. The maximum velocity is located either at the free surface ($U_c = U_{ship} + U_{current}$) when the current is inhibiting ship motion, or at the canal bottom when the current is assisting ship motion ($U_c = U_{ship}$). Adopting this methodology guarantees the time step will be no smaller than the case used in the validation exercise described later.

4.1.4. Modelling sinkage and trim

To model ship sinkage and trim and to detect changes induced by the varying currents, a morphing mesh is imposed in conjunction with the Dynamic Fluid-Body Interaction (DFBI) module of Star-CCM+. At each time step, the DFBI technique computes the forces and moments acting on the hull and adjusts the position of the hull accordingly. The vessel is prevented from morphing the surrounding mesh during the first 5 s of the computational solution to allow the disturbance originating from the impulsive start of the simulation to partially decay and accelerate convergence.

4.1.5. Stopping criteria

To ensure all simulations have achieved adequate convergence, a set of stopping criteria are imposed. A minimum of 250 s of

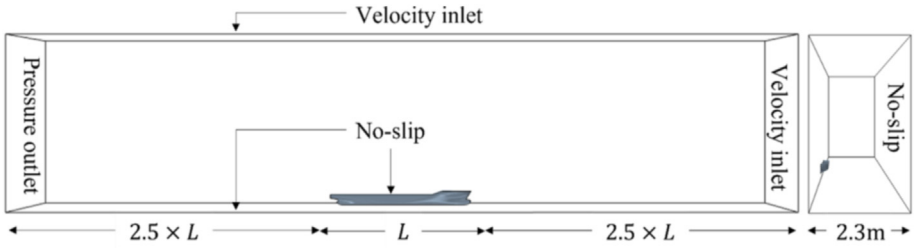

Fig. 1. Computational domain and boundary conditions for all cases ($L = 3.067$ m).

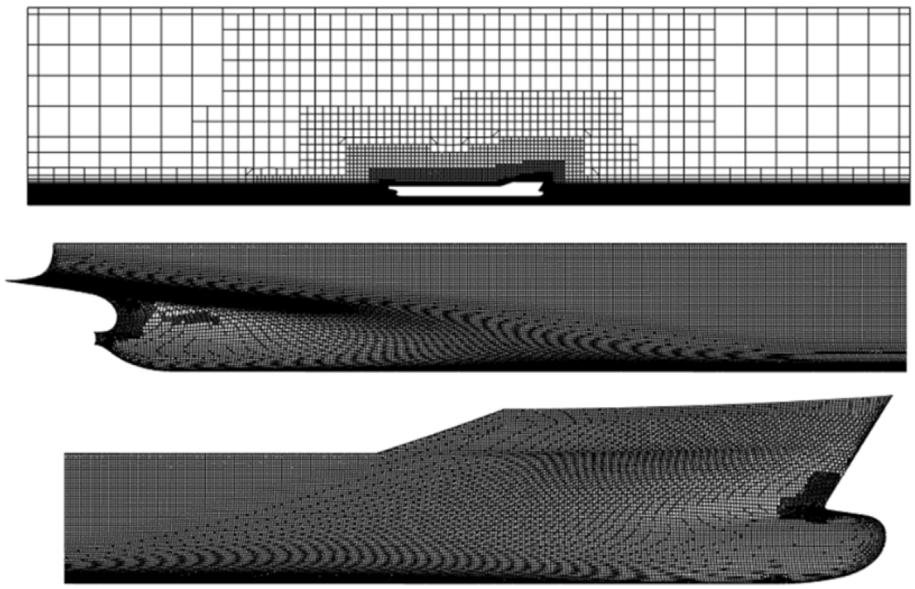

Fig. 2. Depictions of the generated mesh.

physical time is allowed to elapse before stopping the solution. Once this criterion is satisfied, iterative convergence is checked to ensure the resistance time-history is stable and exhibits unsteadiness below 0.1%. This is coupled with an examination of the residuals which are required to reduce by no less than 3 orders of magnitude before a simulation is judged as converged. In all cases, residuals reduced to at least of ~10^{-4}.

4.2. Shear current modelling

When introducing the current within the computational solution it is important to ensure that the depth-dependent shear is modelled correctly and that the correct shape is preserved throughout the virtual towing tank. The purpose of this section is to investigate the performance of the chosen set up by using the numerical environment described above.

As mentioned in the literature review, the presence of the hull creates its own vorticity, so an assessment without that disturbance is necessary. The influence of the vessel is eliminated by removing the ship geometry from the domain while maintain all other mesh and time step characteristics and allowing 2.5 residence times to elapse before comparing the target and achieved shear current shapes. The flow velocity is in all cases chosen as the smallest value of the surface current or the vessel speed. The location chosen to sample the velocity field at the end this simulation (2.5 residence times) is coincident with where the aft perpendicular would be located, that is, 3.5 ship lengths from the inlet boundary.

The flow is introduced in the negative x direction in the case when there is no shear with a constant magnitude, i.e. the flow does not change with distance from the canal wall. Two variations of the current are modelled for each current shape and shear: one assisting ship motion ($U = U_{ship} - U(z)$), and one inhibiting ship motions ($U = U_{ship} + U(z)$). The resulting current shapes and strengths are shown in Fig. 3. The deviations between the target current shapes and strengths listed in Eq. (1), Eq. (2), Eq. (3), and Table 2 are only appreciable near the canal and very close to the water surface. The biggest disagreements are apparent for the 1/7 power law, but since these are located 1 h/T units from the vessel, the disagreement is deemed acceptable.

5. Validation and verification

An estimate of the uncertainty stemming from the mapping of the continuous partial differential governing equations onto discrete intervals in space and time is a key requirement for any numerical work (ASME (American Society of Mechanical Engineers), 2009). To obtain such an estimate, the grid and time step are systematically coarsened by some constant parameter, known as the refinement ratio (r). This gives rise to the fine, medium, and coarse solutions. To obtain the uncertainty, one first performs a verification study, followed by a validation exercise.

The result of the verification exercise is a symmetrical band around the fine solution (the solution obtained using the grid and time step described previously). In this study, these are obtained by systematically coarsening the grid by a factor of $r = \sqrt{2}$ as

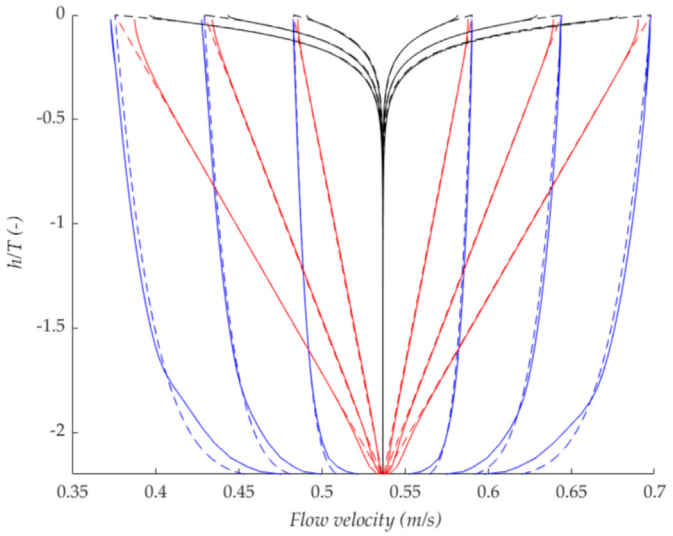

Fig. 3. Current shape and strength and comparison with target equations (Eq. (1), Eq. (2), Eq. (3)). Red: linear current; blue: 1/7 power law currents; black: exponential currents. Dashed lines indicate the target current shapes, while the solid lines indicate the achieved current shape and strength. The data shown is obtained for $Fr_h = 0.303$ ($U_{ship} = 0.537$ m/s). Assisting currents are located to the left of U_{ship}, while inhibiting currents are shown to the right of U_{ship}.

recommended by the ITTC (2008). While coarsening the grid, the Courant number is maintained following the recommendations of Burmester et al. (2020), meaning that the grid and time step are multiplied by the same refinement factor to produce the medium and coarse solution. Once the three simulation results are obtained, the first step is to obtain the difference between the medium-fine and coarse-medium solutions, as shown in Eq. (5) and Eq. (6):

$$\varepsilon_{21} = S_2 - S_1 \tag{5}$$

$$\varepsilon_{32} = S_3 - S_2 \tag{6}$$

where S_1, S_2, S_3 indicate the fine, medium, and coarse solution, respectively. The values obtained from Eq. (5) and Eq. (6) are then used to predict how the solution approaches the asymptotic range through the convergence ratio:

$$R = \varepsilon_{21}/\varepsilon_{32} \tag{7}$$

The value of the convergence ratio dictates if the solution exhibits monotonic convergence ($0 < R < 1$), oscillatory convergence ($-1 < R < 0$), or divergence ($|R| > 1$). In coarsening the grid, the medium and coarse solution were composed of approximately 2,255,626 and 1,126,626, respectively. The observed order of accuracy, an indication of the solution's proximity to the asymptotic range, with the theoretical value $p_t = 2$, is given by:

$$p = \frac{1}{\ln(r_{21})}\left|\ln\left|\varepsilon_{32}\middle/\varepsilon_{21}\right| + q(p)\right| \tag{8}$$

$$q(p) = \ln\left(\frac{r_{21}^p - s}{r_{32}^p - s}\right) \tag{9}$$

and

$$s = \mathrm{sgn}\left(\frac{\varepsilon_{32}}{\varepsilon_{21}}\right) \tag{10}$$

where $r_{21} = r_{32} = \sqrt{2}$, making $q(p) = 0$. When the order of accuracy is known, the so-called Grid Convergence Index (GCI) is estimated through (Celik et al., 2008):

$$GCI = 1.25\left|\frac{S_1 - S_2}{S_1}\right| \Big/ (r_{21}^p - 1), \tag{11}$$

Once the uncertainty estimate is obtained, the validation uncertainty can be estimated, which consists of a root sum of the GCI and experimental uncertainty (Validation uncertainty $= \sqrt{GCI^2 + EFD_{uncertinaty}^2}$). According to Elsherbiny et al. (2019), while the experimental uncertainty is different for resistance, sinkage, and trim, it also depends on the speed. The aforementioned authors specify that low speed uncertainty is 2.2% for resistance and 90% for sinkage and trim because of the relatively small values measured in the experiment (in the range of 1 mm−2 mm), meaning that the values of interest cannot measured reliably. On the other hand, when the speed is high, the resistance uncertainty is 0.79%, the sinkage uncertainty is 3.47%, and the trim uncertainty is 4.46%. Since Elsherbiny et al. (2019) did not specify which depth Froude number should be taken as a cut-off to distinguish between low and high speeds, a validation assessment is made using both categories of uncertainty. For a validation to be successful, the comparison error must be smaller than the validation uncertainty.

The results of the validation and verification exercise results are presented in Table 3. The order of accuracy in the case of resistance and sinkage is reasonably close to the theoretical order of accuracy, p_t, which are also characterised by monotonic convergence. However, the trim results exhibit a behaviour consistent with oscillatory convergence, making the convergence ratio, $R_{trim} = -0.775$. The numerical model shows excellent accuracy in the case of resistance, and very good accuracy in the case of sinkage, but the trim value is underpredicted by approximately 18.7%. This deviation is deemed acceptable because of the small values making up the error (approximately 0.0038 °). Based on the literature review and the results of Terziev et al. (2019), and Bechthold and Kastens (2020) it can be concluded that trim is considerably harder to predict with the same accuracy possible for sinkage and resistance. The latter two parameters are validated in both the low and high uncertainty cases, exhibiting a discretisation uncertainty of 0.961% and 2.836%, respectively. On the other hand, the trim exhibits a discretisation

Table 3
Results from validation and verification study for $Fr_h = 0.303$ Validation and verification was performed with no shear current present.

Quantity	Property		
	Resistance	Sinkage	Trim
Refinement ratio	$\sqrt{2}$	$\sqrt{2}$	$\sqrt{2}$
Fine (S_1)	1.3010 N	0.0020 m	0.0182 °
Medium (S_2)	1.3141 N	0.0021 m	0.0206 °
Coarse S_3	1.3442 N	0.0023 m	0.0175 °
Order of accuracy	2.4123	2.6261	9.094
Convergence ratio	0.4334	0.4025	−0.775
Convergence	*Monotonic*	*Monotonic*	*Oscillatory*
GCI uncertainty	0.961%	2.836%	0.730%
Experimental value	1.301 N	0.0021 m	0.022 °
Comparison error	0.0015%	2.744%	18.700%
High speed experimental uncertainty			
Experimental uncertainty	0.790%	3.470%	4.460%
Validation uncertainty	1.244%	4.481%	4.519%
Validated?	***Yes***	***Yes***	***No***
Low speed experimental uncertainty			
Experimental uncertainty	2.2%	90%	90%
Validation uncertainty	2.401%	90.045%	90.003%
Validated?	***Yes***	***Yes***	***Yes***

uncertainty of 0.73% and is only validated in the low speed case, where the validation uncertainty is approximately 90%.

6. Results and discussion

6.1. Sinkage and trim

This section presents the obtained results and discusses the findings. To begin with, sinkage data for both examined speeds ($Fr_h = 0.303,\ 0.47$) are compared alongside the influence of the current shape and strength in Fig. 4 for $Fr_h = 0.303$ and Fig. 5 for $Fr_h = 0.47$. Here, negative U_0/U_{ship} values denote assisting currents.

Figs. 4 and 5 reveal that sinkage is highly sensitive to the current shape. Inhibiting currents show that for the same flow velocity at the free surface (Fig. 3), the sinkage for $Fr_h = 0.303$ increases by approximately 110%, while for $Fr_h = 0.47$ the sinkage may increase by up to approximately 170% when the current is linear. On the other hand, the 1/7 power current (Eq. (2)) can increase sinkage by no more than 59% for $Fr_h = 0.303$ and 79.3% for $Fr_h = 0.47$. Exponential currents have a comparatively negligible impact on sinkage, registering an increase of no more than 4.5% and 1.5% for the lower and higher speed, respectively.

When the current is assisting ship motion, the overall trend is reversed, but the changes relative U_0 are considerably smaller. Linear assisting currents do not reduce sinkage by more than 55.3% for the low speed examined, and 64.1% in the higher speed case. Similarly, currents following a 1/7 power law do not decrease sinkage by more than 41% and 47% in the low and high-speed cases, respectively. Finally, exponential currents have a tempered effected between 3% and 6%. When varying U_0 at low ship speeds, inhibiting currents tend to vary linearly whereas assisting currents follow approximately a quadratic path, as evidenced by Fig. 4. With increasing speed, this pattern does not hold; Fig. 5 shows that varying U_0/U_{ship} from negative to positive values tends to preserve a quadratic growth.

Fig. 6 and Fig. 7 show that trends observed for sinkage largely hold for trim (denoted θ) as well. The key difference is that trim is more sensitive to the current strength, showing a maximum increase of up to 238% for linear currents, 109% for 1/7 power law currents, and 4.5% for exponential currents when $Fr_h = 0.47$. Similarly to sinkage, trim is affected less when the speed is lower across the current shapes and strengths examined. However, the previously mentioned quadratic pattern across the $U_0/\ U_{ship}$ range is preserved for trim is preserved better for trim than it is for sinkage even for $Fr_h = 0.303$, particularly when the current shape is linear. As pointed out in the literature review section, changes of such magnitude in resistance have been predicted by other researchers (Aalvik, 2019; Benzaquen et al., 2014; Ellingsen, 2014; Li et al., 2019; Li and Ellingsen, 2016a, 2016b).

Trim also exhibits greater sensitivity to exponential currents when compared to sinkage. For example, the CFD model predicts that sinkage can decrease between 2.5% and 6.4% when $U_0/U_{ship} = -0.3$, whereas trim decreases by up to 9.7%. Nevertheless, the magnitude of these changes is comparatively negligible when considering the changes incurred by the linear and 1/7 power law currents. The recorded increases in sinkage and trim as a result of linear inhibiting currents clearly pose a danger of grounding to a vessel and should be considered when selecting the vessel speed. It should however be noted that the sinkage and trim data shown herein were achieved by maintaining the vessel speed regardless of the strength of the current, which will clearly have implications in terms of resistance. These consequences are examined in the following sub-section.

6.2. Resistance

As was the case in sinkage and trim, resistance results are presented for each speed. The dimensional resistance data are made dimensionless by dividing the numerically recorded force by $0.5\,\rho S U_{ship}^2$ (see Table 1), where $\rho = 997.651$ kg/m^3 is the fresh water density. The velocity of the ship is chosen as a baseline in obtaining (U_{ship}) dimensionless values in all cases to ensure consistency.

Fig. 8 and Fig. 9 show the total resistance coefficients (C_T) obtained for all cases. The results show a trend that is similar to that observed for sinkage and trim. Namely, resistance is increased the most by the linear currents despite the volume flux being lower in that case. The linear current may increase by a factor of 2.5 (approximately 150% increase) when $U_0/U_{ship} = 0.3$ for $Fr_h = 0.47$. Therefore, it is unlikely that a ship may be able to sustain the speed over ground (equivalent to $Fr_h = 0.47,\ 0.303$) when the inhibiting current is strong. The exponential current once more shows a comparatively small effect regardless of whether the current is inhibiting or assisting ship motion. These trends are valid for both the $Fr_h = 0.47,\ 0.303$.

The sensitivity of resistance to speed appears to be stronger than

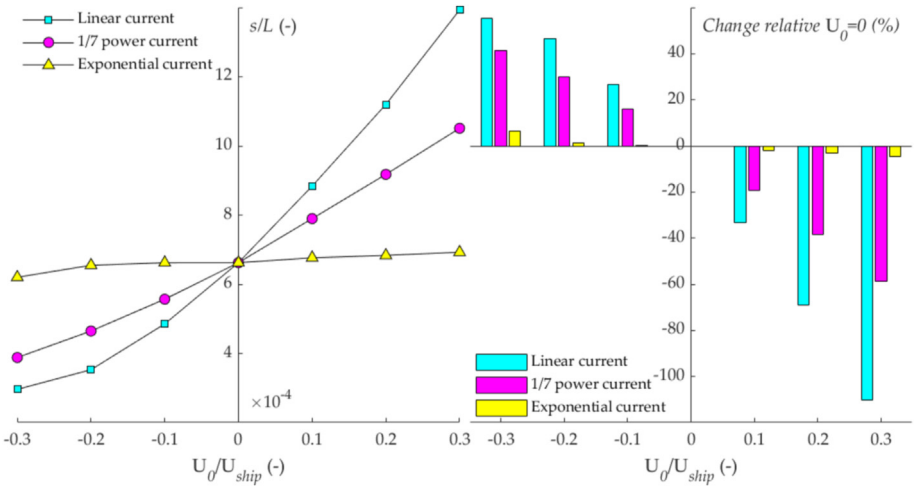

Fig. 4. Sinkage predictions and changes relative U_0 for all current shapes and strengths in the case of $Fr_h = 0.303$.

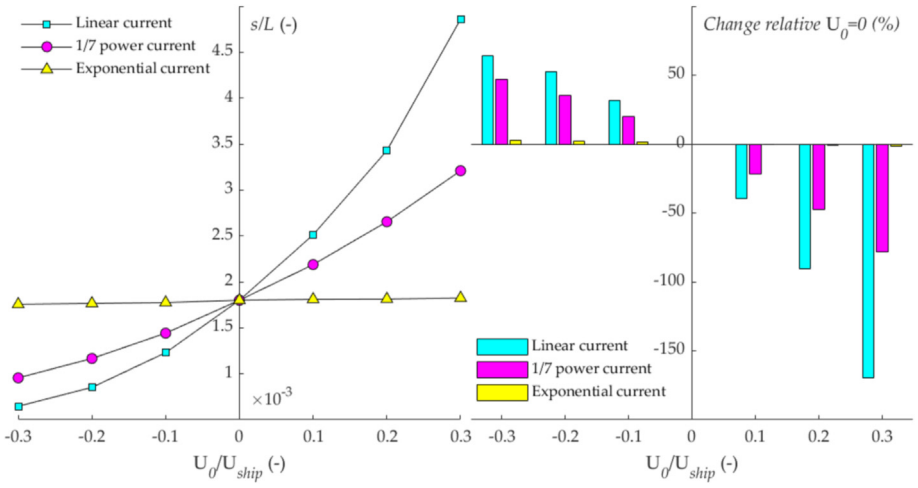

Fig. 5. Sinkage predictions and changes relative U_0 for all current shapes and strengths in the case of $Fr_h = 0.47$.

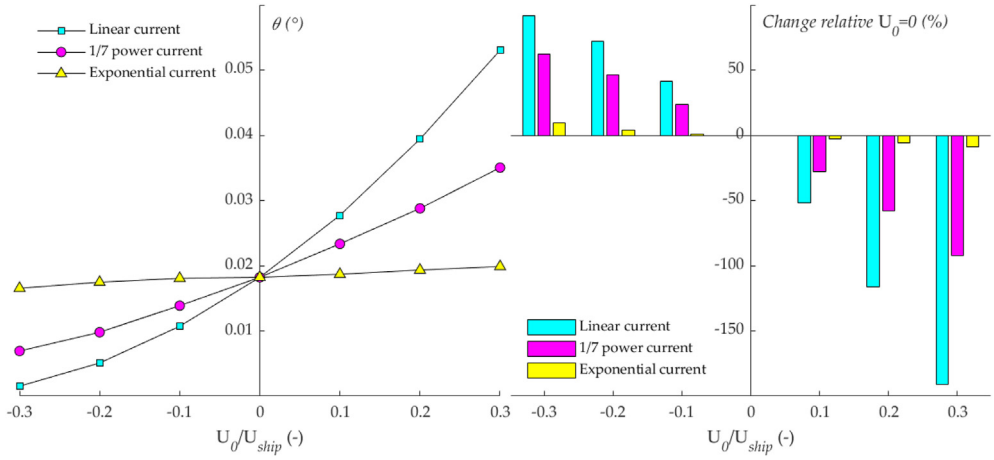

Fig. 6. Trim predictions and changes relative U_0 for all current shapes and strengths in the case of $Fr_h = 0.303$.

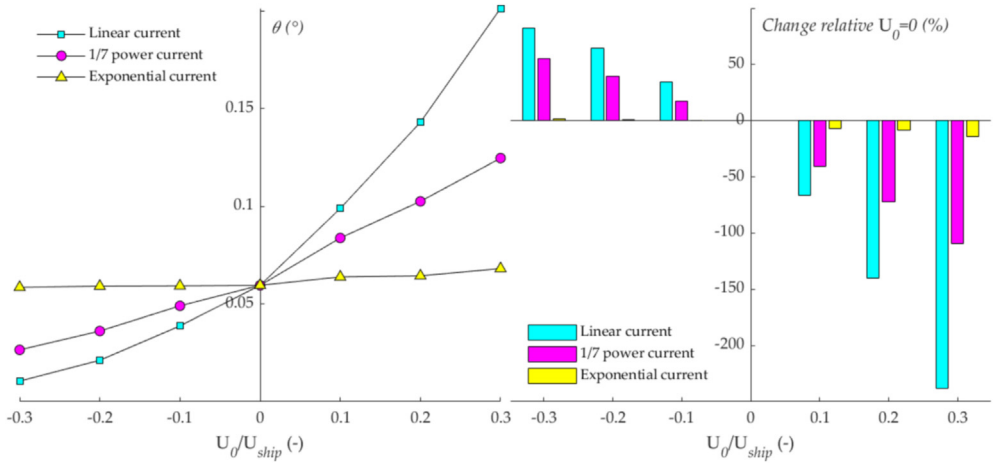

Fig. 7. Trim predictions and changes relative U_0 for all current shapes and strengths in the case of $Fr_h = 0.47$.

in sinkage and trim based on the assisting current results of Fig. 9, where approximate quadratic pattern is broken. Additionally, the reductions in resistance when the currents are assisting ship motion are higher than they are for sinkage and trim. When the depth Froude number is 0.303 ($h/T = 2.22$), the linear current can reduce the resistance by up to approximately 75% when $U_0/U_{ship} = 0.3$. Similarly, the 1/7 power current may reduce the resistance by 47%, while the exponential current can achieve a reduction in the region

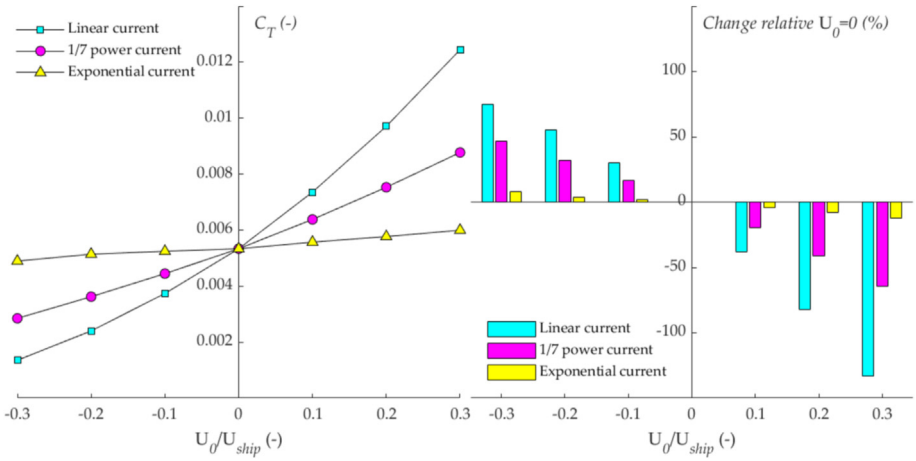

Fig. 8. Total resistance coefficients and changes relative U_0 for all current shapes and strengths in the case of $Fr_h = 0.303$.

of 8%. When the speed is higher, the relative differences are also higher: up to 96% for linear currents, 48% for 1/7 power currents, and 2% for exponential currents.

The above results point to the fact that significant fuel efficiency may be possible if currents are exploited to schedule ship departure and arrival where confined water subject to currents are involved. The final aspect of the solution presented is the wave fields produced by the hull, shown in Fig. 10 for assisting currents and Fig. 11 for inhibiting currents. Since lower speeds are more likely to be realistic in confined waterways, attention is focused to the lower depth Froude number, $Fr_h = 0.303$. The results show that assisting currents reduce the magnitude of the near-field disturbance generated by the vessel, while inhibiting currents have a magnifying effect. Linear and 1/7 power law currents also cause far-field waves to be shed from the ship.

7. Conclusion

A numerical investigation to establish the impact of sheared currents on ship hydrodynamics was performed using a commercially available URANS solver. A validation and verification exercise for a case without a shear current showed the numerical model is validated in terms of resistance, exhibiting a negligible error and a discretisation uncertainty of 0.961%. Sinkage was also validated, showing an uncertainty of 2.836%, however, trim was only validated when the high experimental uncertainty (Elsherbiny et al., 2019) is taken into account despite exhibiting a numerical uncertainty of 0.730%.

Three depth-varying current shapes were investigated: linear, 1/7 power law, and exponential. Three current strengths, equivalent to 10%, 20%, and 30% of the ship speed were applied for inhibiting and assisting currents. Despite the differences in volume flux, the linear current showed the greatest increase in resistance, sinkage and trim of the benchmark hull in confined water when the current assists ship motion. Similarly, when the current inhibits ship motion, the linear current showed the highest increase in all parameters.

When the current is linear and assists ship motion resistance can decrease between 75% and 96% for $Fr_h = 0.303$ and $Fr_h = 0.47$, respectively. Sinkage and trim are predicted to be less sensitive to the current, decreasing by between 55% and 64%. When the linear current inhibits ship motion, the predicted increases are in the range of 100%–200% in all parameters for $U_0/U_{ship} = 0.3$, highlighting the current can have profound impacts on the energy efficiency of a hull. Similar results have been predicted by other researchers (Aalvik, 2019; Benzaquen et al., 2014; Ellingsen, 2014; Li et al., 2019; Li and Ellingsen, 2016a, 2016b). Interestingly, the exponential current showed relatively little change in comparison,

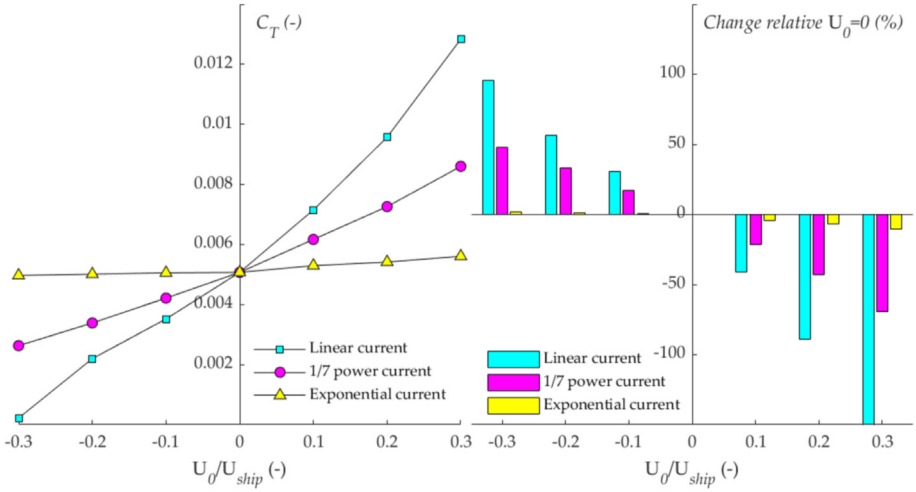

Fig. 9. Total resistance coefficients and changes relative U_0 for all current shapes and strengths in the case of $Fr_h = 0.47$.

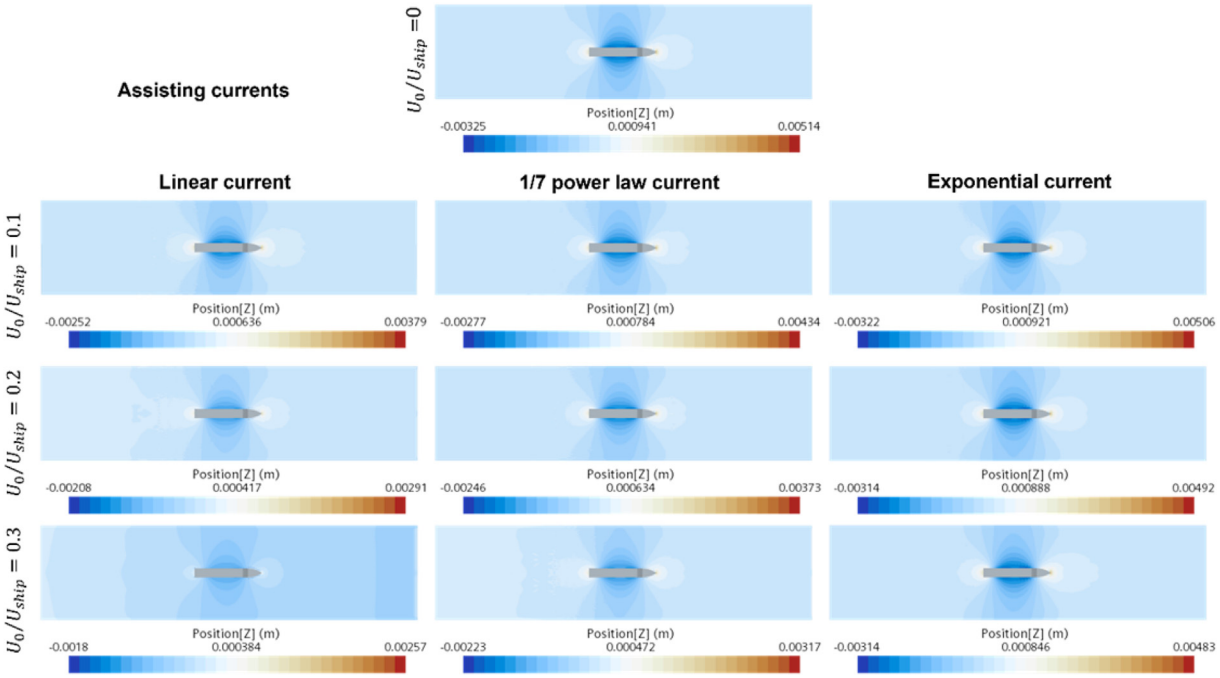

Fig. 10. Free surface patterns produced by the assisting currents for $Fr_h = 0.303$.

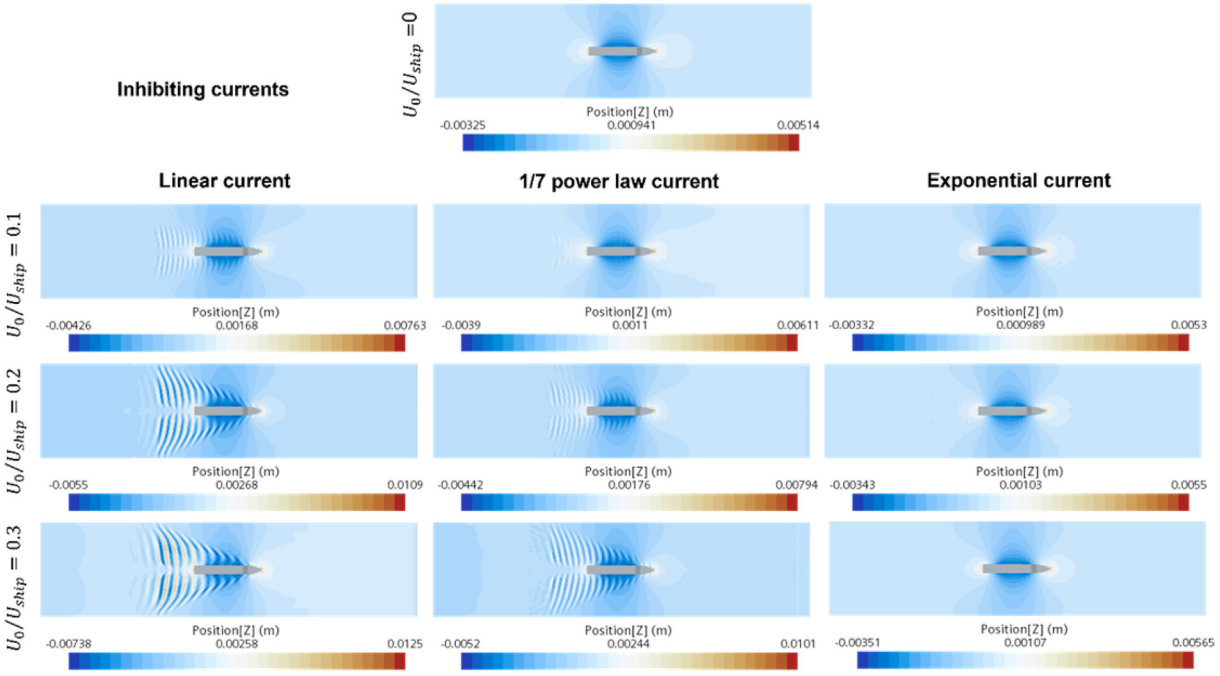

Fig. 11. Free surface patterns produced by the inhibiting currents for $Fr_h = 0.303$.

with a maximum increase of 9.7% in trim. As was the case for other currents, when the exponential current assists ship motion, the relative reductions are considerably smaller, typically less than 5% for all parameters. The wave field was shown to vary considerably: the predominantly near-field disturbance generated by the hull at the low depth Froude number was shown to produce far-field waves when subjected to strong currents.

The results described above point to the possibility of significant fuel savings depending on the current shape and strength. The departure and transit times of vessels may be optimised based on local tides, or based on meteorological conditions if these are known to create currents in confined waterways with limited fetch where wind waves are typically absent. The work carried out herein can be extended by varying the water depth and canal width to estimate the effects of the geometrical properties of the waterway. Additionally, more complex current shapes can be modelled. For example, the flow direction may be changed with depth if a weak tide acts against a strong wind.

Declaration of competing interest

The authors declare that they have no known competing financial interests or personal relationships that could have appeared to influence the work reported in this paper.

Acknowledgements

Results were obtained using the ARCHIE-WeSt High-Performance Computer (www.archie-west.ac.uk) based at the University of Strathclyde. The authors gratefully acknowledge that the research presented in this paper was carried out as part of the EU funded H2020 project, VENTuRE (grant no. 856887). All data underpinning this publication are openly available from the University of Strathclyde KnowledgeBase at https://doi.org/10.15129/c1e54193-bc62-4caf-ab9a-fc0ed116a377.

References

Aalvik, E., 2019. Numerical Implementation of the Pressure-Patch Model of Ships on Flows of Arbitrary Shear Profiles. Norwegian University of Science and Technology.

Abdullah, A.J., 1949. Wave motion at the surface of a current which has an exponential distribution of vorticity. Ann. N. Y. Acad. Sci. 51, 425–441. https://doi.org/10.1111/j.1749-6632.1949.tb27282.x.

ASME (American Society of Mechanical Engineers), 2009. Standard for verification and validation in computational fluid Dynamics and heat transfer - ASME V&V 20-2009. ASME Int. 20.

Bechthold, J., Kastens, M., 2020. Robustness and quality of squat predictions in extreme shallow water conditions based on RANS-calculations. Ocean Eng. 197, 106780. https://doi.org/10.1016/j.oceaneng.2019.106780.

Beck, R.F., 1971. Wave resistance of a thin ship with a rotational wake. J. Ship Res. 15, 196–216.

Benzaquen, M., Darmon, A., Raphaël, E., 2014. Wake pattern and wave resistance for anisotropic moving disturbances. Phys. Fluids 26. https://doi.org/10.1063/1.4896257.

Brard, R., 1970. Viscosity, wake, and ship waves. J. Ship Res. 14, 1–34.

Bretherton, F.P., Garret, C.I.R., 1968. Wavetrains in inhomogeneous moving media. Proc. R. Soc. A Math. Phys. Eng. Sci. 302, 529–554. https://doi.org/10.1007/978-3-642-87025-5_18.

Burmester, S., Vaz, G., el Moctar, O., 2020. Towards credible CFD simulations for floating offshore wind turbines. Ocean Eng. 209, 107237. https://doi.org/10.1016/j.oceaneng.2020.107237.

Burns, J.C., 1953. Long waves in running water. Math. Proc. Camb. Phil. Soc. 49, 695–706. https://doi.org/10.1017/S0305004100028899.

Castiglione, T., He, W., Stern, F., Bova, S., 2014. URANS simulations of catamaran interference in shallow water. J. Mar. Sci. Technol. 19, 33–51. https://doi.org/10.1007/s00773-013-0230-5.

Celik, I.B., Ghia, U., Roache, P.J., Freitas, C., 2008. Procedure for estimation and reporting of uncertainty due to discretization in CFD applications. J. Fluid Eng. 130, 078001. https://doi.org/10.1115/1.2960953.

Choi, H., Kim, D.J., Kim, Y.G., Yeo, D.J., Yun, K., Lee, G.J., 2019. An experimental study on dynamic response of geotextile structures in regular waves. In: 5th MASHCON International Conference on Ship Manoeuvring in Shallow and Confined Water. https://doi.org/10.1016/j.proeng.2015.08.372. Ostend, Belgium.

Chun, H.H., Park, I.R., Lee, S.K., 2001. Analysis of turbulence free-surface flow around hulls in shallow water channel by a level-set method. In: Twenty-Second Symposium on Naval Hydrodynamics Office of Naval Research Bassin d'Essais Des. CarenesNational Research Council, pp. 941–956. https://doi.org/10.17226/9771.

Crapper, G.D., 1972. Nonlinear gravity waves on steady non-uniform currents. J. Fluid Mech. 52, 713–724. https://doi.org/10.1017/S0022112072002721.

De Luca, F., Mancini, S., Miranda, S., Pensa, C., 2016. An extended verification and validation study of CFD simulations for planing hulls. J. Ship Res. 60, 101–118. https://doi.org/10.5957/josr.60.2.160010.

Ekman, V.W., 1905. On the Influence of the Earth's Rotation on Ocean-Currents. https://doi.org/10.1016/0022-1236(71)90006-1.

Ellingsen, S., 2014. Ship waves in the presence of uniform vorticity. J. Fluid Mech. 742, 1–11. https://doi.org/10.1017/jfm.2014.28.

Ellingsen, S., Brevik, I., 2014. How linear surface waves are affected by a current with constant vorticity. Eur. J. Phys. 35. https://doi.org/10.1088/0143-0807/35/2/025005.

Ellingsen, S., Li, Y., 2017. Approximate dispersion relations for waves on arbitrary shear flows. J. Geophys. Res. Ocean. 122, 9889–9905. https://doi.org/10.1002/2017JC012994.

Eloot, K., Vantorre, M., Delefortrie, G., Lataire, E., 2016. Running sinkage and trim of the DTC container carrier in harmonic sway and yaw motion : open model test data for validation purposes. Proc. 4th MASHCON, 2016, Hamburg, Ger 251–261. https://doi.org/10.18451/978-3-939230-38-0.

Elsherbiny, K., Tezdogan, T., Kotb, M., Incecik, A., Day, S., 2019. Experimental analysis of the squat of ships advancing through the New Suez Canal. Ocean Eng. 178, 331–344. https://doi.org/10.1016/j.oceaneng.2019.02.078.

Evans, J.T., 1956. Pneumatic and similar breakwaters. Proc. Inst. Civ. Eng. 5, 91–93. https://doi.org/10.1680/ipeds.1956.11769.

Gargett, A.E., Hughes, B.A., 1972. On the interaction between surface and internal waves. J. Fluid Mech. 52, 179–191. https://doi.org/10.3938/jkps.51.616.

Graefe von, A., Shigunov, V., el Moctar, O., 2015. Rankine source method for ship-ship interaction problems. J. Offshore Mech. Arctic Eng. 137, 1–10. https://doi.org/10.1115/1.4029316.

Holliday, D., 1973. Nonlinear gravity–capillary surface waves in a slowly varying current. J. Fluid Mech. 57, 797–802. https://doi.org/10.1017/S0022112073002028.

Hunt, J.N., 1955. Gravity waves in flowing water. Proc. R. Soc. A Math. Phys. Eng. Sci. 231, 496–504.

ITTC, 2014. ITTC – recommended procedures and guidelines - practical guidelines for ship CFD applications. 7.5-03-02-03 (revision 01). ITTC – Recomm. Proced. Guidel. 19.

ITTC, 2008. Uncertainty analysis in CFD verification and validation methodology and procedures. 25th ITTC 2008, Resist. Comm. 12.

Kok, Z., Duffy, J., Chai, S., Jin, Y., 2020. Multiple approaches to numerical modeling of container ship squat in confined water. J. Waterw. Port, Coast. Ocean Eng. 146, 04020017. https://doi.org/10.1061/(asce)ww.1943-5460.0000580.

Li, Y., Ellingsen, S., 2016a. Ship waves on uniform shear current at finite depth: wave resistance and critical velocity. J. Fluid Mech. 791, 539–567. https://doi.org/10.1017/jfm.2016.20.

Li, Y., Ellingsen, S.A., 2016b. Effect of anisotropic shape on ship wakes in presence of shear current of uniform vorticity. Proc. Int. Conf. Offshore Mech. Arct. Eng. - OMAE 7, 1–8. https://doi.org/10.1115/OMAE2016-54250.

Li, Y., Smeltzer, B.K., Ellingsen, S., 2019. Transient wave resistance upon a real shear current. Eur. J. Mech. B Fluid 73, 180–192. https://doi.org/10.1016/j.euromechflu.2017.08.012.

Longuet-Higgins, M.S., Stewart, R.W., 1964. Radiation stresses in vater waves; a physical discussion, with applications. Deep Sea Res. 11, 529–562. https://doi.org/10.1109/TIE.2012.2208438.

Longuet-Higgins, M.S., Stewart, R.W., 1962. Radiation stress and mass transport in gravity waves, with application to 'surf beats. J. Fluid Mech. 13, 481–504. https://doi.org/10.1017/S0022112062000877.

Longuet-Higgins, M.S., Stewart, R.W., 1961. The changes in the form of short gravity waves on long waves and tidal currents. J. Fluid Mech. 10, 565–583. https://doi.org/10.1017/S0022112060000803.

Longuet-Higgins, M.S., Stewart, R.W., 1960. Changes in the form of short gravity waves on long waves and tidal currents. J. Fluid Mech. 8, 565–583. https://doi.org/10.1017/S0022112060000803.

Mucha, P., Deng, G., Gourlay, T., Moctar, O. el, 2016. Validation studies on numerical prediction of ship squat and resistance in shallow water. In: Proc. 4th MASHCON 83–92. https://doi.org/10.18451/978-3-939230-38-0.

Peregrine, D.H., 1976. Interaction of water waves and currents. Adv. Appl. Mech. 16, 9–117. https://doi.org/10.1016/S0065-2156(08)70087-5.

Peregrine, D.H., 1971. A ship's waves and its wake. J. Fluid Mech. 49, 353–360. https://doi.org/10.1017/S0022112071002118.

Prakash, S.M.N., Chandra, B., 2013. Numerical estimation of shallow water resistance of a river-sea ship using CFD. Int. J. Comput. Appl. 71, 33–40. https://doi.org/10.5120/12357-8670.

Razgallah, I., Kaidi, S., Smaoui, H., Sergent, P., 2018. The impact of free surface modelling on hydrodynamic forces for ship navigating in inland waterways: water depth, drift angle, and ship speed effect. J. Mar. Sci. Technol. 1–22. https://doi.org/10.1007/s00773-018-0566-y.

Rotteveel, E., Hekkenberg, R., van der Ploeg, A., 2017. Inland ship stern optimization in shallow water. Ocean Eng. 141, 555–569. https://doi.org/10.1016/j.oceaneng.2017.06.028.

Sakamoto, N., Wilson, R.V., Stern, F., 2007. Reynolds-averaged Navier-Stokes simulations for high-speed wigley hull in deep and shallow water. J. Ship Res. 51, 187–203.

Siemens, 2018. Star-CCM+ User Guide Version 13.04.

Skop, R.A., 1987. Approximate dispersion relation for wave-current interactions. J. Waterw. Port, Coast. Ocean Eng. 113, 187–195. https://doi.org/10.1061/(asce)0733-950x(1987)113:2(187).

Skop, R.A., Leipold, Y., 1988. Modification of directional wave number spectra by surface currents. Ocean Eng. 15, 585–602. https://doi.org/10.1016/0029-8018(88)90003-0.

Söding, H., Von Graefe, A., El Moctar, O., Shigunov, V., 2012. Rankine source method for seakeeping predictions. In: Proceedings of the International Conference on Offshore Mechanics and Arctic Engineering - OMAE, pp. 449–460. https://doi.org/10.1115/OMAE2012-83450.

Tabaczek, T., 2008. Computation of flow around inland waterway vessel in shallow water. Arch. Civ. Mech. Eng. 8, 97–105. https://doi.org/10.1016/S1644-9665(12)60269-6.

Tatinclaux, B.J., 1970. Effect of a rotational wake on the wavemaking resistance of an ogive. J. Ship Res. 14, 84–99.

Taylor, G., 1955. The action of a surface current used as a breakwater. Proc. R. Soc. London. Ser. A. Math. Phys. Sci. 231, 466–478. https://doi.org/10.1098/rspa.1955.0188.

Terziev, M., Tezdogan, T., Incecik, A., 2021. A numerical assessment of the scale effects of a ship advancing through restricted waters. Ocean Eng. 229, 108972.

https://doi.org/10.1016/j.oceaneng.2021.108972.
Terziev, M., Tezdogan, T., Incecik, A., 2020. Application of eddy-viscosity turbulence models to problems in ship hydrodynamics. Ships Offshore Struct. 15. https://doi.org/10.1080/17445302.2019.1661625.
Terziev, M., Tezdogan, T., Incecik, A., 2019. Application of eddy-viscosity turbulence models to problems in ship hydrodynamics. Ships Offshore Struct. 1–24. https://doi.org/10.1080/17445302.2019.1661625.
Terziev, M., Tezdogan, T., Oguz, E., Gourlay, T., Demirel, Y.K., Incecik, A., 2018. Numerical investigation of the behaviour and performance of ships advancing through restricted shallow waters. J. Fluid Struct. 76, 185–215. https://doi.org/10.1016/j.jfluidstructs.2017.10.003.
Thompson, P.D., 1949. The propagation of small surface disturbances through rotational flow. Ann. Nucl. Energy 41, 463–474. https://doi.org/10.1111/j.1749-6632.1949.tb27285.x.
Tuck, E.O., 1966. Shallow-water flows past slender bodies. J. Fluid Mech. 26, 81–95. https://doi.org/10.1017/S0022112066001101.
Unna, P., 1947. Sea waves. Nature 159, 239–242. https://doi.org/10.1038/159239a0.
Wilcox, D.C., 2008. Formulation of the k-w turbulence model revisited. AIAA J. 46, 2823–2838. https://doi.org/10.2514/1.36541.
Yao, J.X., Zou, Z.J., Wang, H.M., 2011. Numerical study on bank effects for a ship sailing in shallow channel. J. Shanghai Jiao Tong Univ. (Sci.) 16, 91–96. https://doi.org/10.1007/s12204-011-1100-0.
Yoshida, K., 1952. Dynamics on the Co-existent system of waves and currents in the ocean. Part 1. J. Oceanogr. Soc. Jpn. 7, 97–104.
Zeng, Q., Hekkenberg, R., Thill, C., 2019. On the viscous resistance of ships sailing in shallow water. Ocean Eng. 190, 106434. https://doi.org/10.1016/j.oceaneng.2019.106434.
Zeng, Q., Thill, C., Hekkenberg, R., Rotteveel, E., 2018. A modification of the ITTC57 correlation line for shallow water. J. Mar. Sci. Technol. 24 (2). https://doi.org/10.1007/s00773-018-0578-7.
Zwijnsvoorde, T. Van, Ruiz, M.T., Lataire, E., 2018. Sailing in shallow water waves with the DTC container carrier: open model test data for validation purposes. In: International Conference on Ship Manoeuvring in Shallow and Confined Water. Ostend, Belgium.